A Performance Analysis of Trellis-Coded Modulation Schemes Over Rician Fading Channels

Chinthananda Tellambura, Qiang Wang, and Vijay K. Bhargava, *Fellow, IEEE*

***Abstract*— This paper presents a saddle point approximation (SAP) method to compute the pairwise error probability (PEP) of trellis-coded modulation (TCM) schemes over Rician fading channels. The approximation is applicable under several conditions, such as finite and ideal interleaving, ideal coherent and pilot-tone aided detection, and differential detection. The accuracy of this approximation is demonstrated by comparison to the results of numerical integration. When ideal interleaving is assumed, an asymptotic approximation for the PEP of ideal coherent, pilot-tone aided or differentially detected TCM is derived. This asymptotic approximation of the PEP is in a product form and much tighter than the ordianry Chernoff bound on the PEP. Also, based on the SAP, the effect of finite interleaving depth on the error performance of TCM schemes over Rician and shadowed Rician channels is studied.**

I. Introduction

TO MITIGATE the effects of fading, trellis-coded modulation (TCM) schemes have been proposed for fading channels (e.g., mobile satellite and cellular mobile systems) [1]. Typically, the analytical performance evaluation of such systems has been limited to upper bounds and ideal interleaving. Due to their looseness, upper bounds based on the Chernoff bound only yield qualitative descriptions of error performance. Accurate results must be obtained by computer simulation. In order to obtain improved analytical estimates, Cavers and Ho [2] have proposed a method to compute the exact pairwise error probability (PEP) of trellis-coded multilevel phase shift keying (TC-MPSK) and multilevel differential phase shift keying (TC-MDPSK) over ideally interleaved Rayleigh fading channels. Ho and Fung [3] have extended the results of [2] to nonideally interleaved Rayleigh fading channels. The residue method proposed in [2], [3] does not apply in the case of Rician fading channels. To remedy this situation, Huang and Campbell [4] have derived a saddle-point approximation (SAP) for the exact PEP of TC-MDPSK over nonideally interleaved Rician and shadowed Rician fading channels.

In this paper, we derive the approximate PEP of both TC-MPSK (ideal or pilot-tone based) and TC-MDPSK over Rician type fading channels, including both ideal and nonideal interleaving. Our approximation is based on the saddle point method [5], [6], [7], and the accuracy of this approximation is confirmed by comparing it to the results of numerical integration. We then apply the approximate PEP to evaluate the performance of TC-MPSK and TC-MDPSK schemes. Both schemes are studied for Rician channels [1], and the effects of non-ideal interleaving are taken into account. TC-MDPSK over shadowed Rician channels [8] is also studied, taking into consideration the effects of nonideal and ideal interleaving. When ideal interleaving is employed to combat the fading (the interleaving depth sufficiently large for this requirement will be given later in this paper), an asymptotic approximation to the PEP of TC-MPSK (ideal or pilot-tone based) and TC-MDPSK over Rician fading channels is derived. It leads directly to a union upper bound on the bit error probability via the transfer function bounding technique. Also, it resembles the well-known Chernoff bound [1] for the PEP and differs only by a multiplying factor that improves the approximation.

The paper is organized as follows. Section II describes the system model used here and the characterization of Rician and shadowed Rician fading channels. A saddle-point approximation to the PEP of TC-MPSK and TC-MDPSK is derived in Section III. Several examples are presented in Section IV. Finally, conclusions are provided in Section V.

II. SystemModel

We consider a typical system model [1], [9] as shown in Fig. 1. Binary input data are convolutionally encoded at rate $n/(n+1)$. The encoded $n+1$ bit words are block interleaved and mapped into a sequence $x = (\hat{x}_1, \hat{x}_2, \cdots, \hat{x}_N)$ of M-ary PSK symbols, which constitute a normalized constellation, i.e., $|x_k|^2 = 1$ for all symbols. For TC-MDPSK, additional differential encoding/decoding is performed as shown in Fig. 1. The receiver deinterleaves and then applies soft-decision Viterbi decoding. Here, we consider a block interleaver of N_s columns (interleaving span) and N_d (interleaving depth) rows of memory. The encoder output is written into the memory row by row and then read out column by column. The received symbols are reordered in the reverse manner.

The transmitted signal is represented in the baseband as [2]

$$e(t) = \sum_{-\infty}^{\infty} v_{k'} s(t - k'T_s) \tag{1}$$

where $s(t)$ is a unit-energy pulse that satisfies Nyquist's conditions for zero intersymbol interference, T_s is the symbol duration, and

$$v_{k'} = \begin{cases} x_k, & \text{TC-MPSK} \\ v_{k'-1}x_k, & \text{TC-MDPSK} \end{cases} \tag{2}$$

where x_k denotes the kth convolutional encoder output. Because of interleaving, the transmitted signal corresponding to

Manuscript received September 4, 1992; revised November 5, 1992.

The authors are with the Department of Electrical and Computer Engineering, University of Victoria, B.C., Canada V8W 3P6.

IEEE Log Number 9208470.

0018–9545/93$03.00 © 1993 IEEE

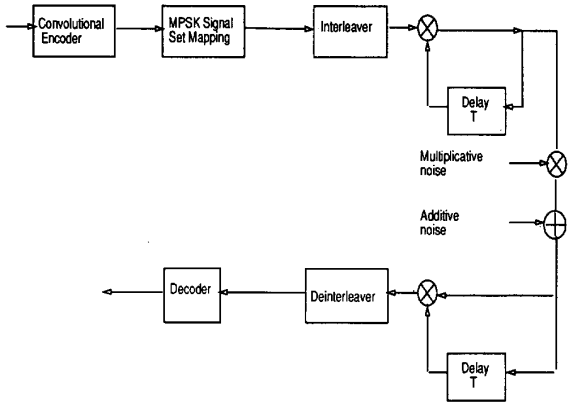

Fig. 1. Baseband system model where T is the symbol period.

x_k is transmitted as the k'th term of the transmitted sequence, as indicated in (1). In the case of ideal interleaving, this prime superscript will be omitted.

The signal is demodulated using a filter matched to $s(t)$. Hence, the received sample corresponding to the kth coded symbol can be denoted by

$$y_{k'} = \alpha_{k'} v_{k'} + n_{k'} \tag{3}$$

where $n_{k'}$ is a complex-Gaussian random variable with zero mean and variance $\sigma^2 = (2\gamma_s)^{-1}$, where $\gamma_s = \overline{E}_s/N_0$. The channel gain $\alpha_{k'}$ is modeled as a complex-Gaussian random variable having statistical parameters.

$$\langle \alpha_{k'} \rangle = A, \qquad \tfrac{1}{2}\langle (\alpha_{k'} - A)(\alpha_{k'} - A)^* \rangle = b_0 \tag{4}$$

where the constant mean A denotes the line of sight (LOS) and specular components of the received signal, and b_0 is the variance of the diffuse component (Rayleigh fading) of the received signal. The normalizations $A^2 + 2b_0 = 1$ and $K = A^2/2b_0$ enable the Rician channel to be characterized by a single parameter K. For shadowed Rician fading, A is a lognormally distributed random variable having the probability density function

$$p(x) = \begin{cases} \dfrac{1}{\sqrt{2\pi d_0}x} \exp\left(-\dfrac{(\log(x) - \mu_0)^2}{2d_0}\right), \\ \qquad x > 0 \\ 0, \qquad \text{elsewhere.} \end{cases} \tag{5}$$

The shadowing model parameters are from [8]. In the following section, the SAP for the PEP of a TCM scheme will be introduced.

III. PairwiseError Probability

As in [2], we take the Viterbi decoder metric to be Euclidean, i.e.,

$$m(y_{k'}, x_k) = -|y_{k'} - \beta \hat{\alpha}_{k'} x_k|^2 \tag{6}$$

where $\hat{\alpha}_{k'}$ is the estimate of the true channel gain $\alpha_{k'}$. $\beta = \mu\sqrt{b_0/b_1}$, where b_1 and μ are the variance of $\hat{\alpha}_{k'}$ and the normalized correlation coefficient between $\hat{\alpha}_{k'}$ and $\alpha_{k'}$, respectively. Depending on the detection technique used, the estimate $\hat{\alpha}_{k'}$ is obtained as follows:

$$\hat{\alpha}_{k'} = \begin{cases} \alpha_{k'}, & \text{TC-MPSK} \\ y_{k'-1}, & \text{TC-MDPSK} \\ \alpha_{k'} + \zeta_{k'}, & \text{TC-MPSK with a pilot} \end{cases} \tag{7}$$

where $\zeta_{k'}$ is the additive noise term, appearing because of the nonzero bandwidth of the pilot-tone extraction filter. This will be considered later. We remark that decoding with the first estimate is optimal (i.e. in a maximum-likelihood sense) but unachieveable while the last two are nonoptimal but easily implementable.

The PEP $P(x \to \hat{x})$ is defined to be the probability of choosing the coded sequence $\hat{x} = (\hat{x}_1, \hat{x}_2, \cdots, \hat{x}_N)$ when in reality $x = (x_1, x_2, \cdots, x_N)$ was transmitted [1]. Since, of the two coded symbol sequences, only the components that differ contribute to the PEP, assign the set of subscripts $k_i, (i = 1, 2, \cdots, L)$, arranged in ascending order, for which $x_{k_i} \neq \hat{x}_{k_i}$. Note that L is the Hamming distance between x and $\hat{x}$. The smallest possible $L, L_{\min}$, is known as the code *diversity*. The PEP, by using the fact that the total metric for a codeword is the sum of component metrics, is

$$P(x \to \hat{x}) = \Pr\{\xi < 0\} \tag{8}$$

where

$$\xi = \sum_{i=1}^{L} y_{k_i'} \beta^* \hat{\alpha}_{k_i'}^* (x_{k_i} - \hat{x}_{k_i})^* + y_{k_i'}^* \beta \hat{\alpha}_{k_i'} (x_{k_i} - \hat{x}_{k_i}). \tag{9}$$

Let V_i denote the 2×1 column matrix

$$V_i = (\hat{\alpha}_{k_i'} \quad y_{k_i'})^T. \tag{10}$$

Thus the decision variable ξ can be compactly represented as

$$\xi = \sum_{i=1}^{L} V_i^\dagger F_i V_i = \boldsymbol{F}^\dagger \boldsymbol{F} \boldsymbol{V} \tag{11}$$

where the dagger denotes conjugate transpose, and $\boldsymbol{V}$, $\boldsymbol{F}$ are given by

$$\boldsymbol{V} = \begin{pmatrix} V_1 \\ \vdots \\ V_L \end{pmatrix}, \qquad \boldsymbol{F} = \begin{pmatrix} F_1 & \cdots & 0 \\ \vdots & \ddots & \vdots \\ 0 & \cdots & F_L \end{pmatrix} \tag{12}$$

with

$$F_i = \begin{pmatrix} 0 & \beta^*(x_{k_i} - \hat{x}_{k_i})^* \\ \beta(x_{k_i} - \hat{x}_{k_i}) & 0 \end{pmatrix}. \tag{13}$$

From (3), (4), and (10), it follows that each V_i is Gaussian with the 2×2 covariance matrix

$$R_i = \begin{pmatrix} b_1 & \mu\sqrt{b_0 b_1} x_{k_i} \\ \mu^*\sqrt{b_0 b_1} x_{k_i}^* & b_0 + \sigma^2 \end{pmatrix}. \tag{14}$$

For the two cross-correlation terms in this, x_{k_i}, appears instead of $v_{k_i'}$, as necessitated by (3), because for TC-MDPSK the term $\alpha_{k_i'} v_{k_i'-1}$ is considered the true channel gain. We also need the covariance matrix $\boldsymbol{R}$ of the random vector $\boldsymbol{V}$. $\boldsymbol{R}$ is defined as the $2L \times 2L$ matrix

$$\boldsymbol{R} = \tfrac{1}{2}\langle [\boldsymbol{V} - \langle \boldsymbol{V} \rangle]^* [\boldsymbol{V} - \langle \boldsymbol{V} \rangle]^T \rangle. \tag{15}$$

Next we obtain an SAP to the PEP given by (8).

A. The SAP

From (8), the PEP is

$$P(x \to \hat{x}) = \Pr(\xi < 0) = \int_{-\infty}^{0} p_\xi(\xi)\, d\xi. \tag{16}$$

In terms of the characteristic function $G_\xi(\nu)$ of ξ, the above can be expressed as [4]

$$P(x \to \hat{x}) = \frac{-1}{2\pi j} \int_{-\infty+j\epsilon}^{\infty+j\epsilon} \frac{G_\xi(\nu)}{\nu} d\nu \tag{17}$$

where $\epsilon > 0$, to avoid the singularity at the origin. The characteristic function of ξ is given by [10, App. B]

$$G_\xi(\nu) = \frac{\exp\left(j\nu \langle \boldsymbol{V} \rangle^\dagger (\boldsymbol{F}^{-1} - 2j\nu \boldsymbol{R}^*)^{-1} \langle \boldsymbol{V} \rangle\right)}{\det(\boldsymbol{I} - 2j\nu \boldsymbol{R}^* \boldsymbol{F})} \tag{18}$$

where $\boldsymbol{V}, \boldsymbol{R}, \boldsymbol{F}$ are defined above. Except for the case of Rayleigh fading, the above integral appears to defy an analytical solution. It is, however, not difficult to compute the above integral numerically, as the absolute value of the integrand can be made to decrease to zero quickly as $|\nu| \to \infty$ by choosing a suitable ϵ. Nevertheless, it is desirable to avoid the numerical integration of (17) and find an efficient and accurate alternative. Therefore, we turn to the SAP method for this type of contour integral [5], [7], [6].

As substituting $s = j\nu$, (17) can be converted to an equivalent contour integral

$$P(x \to \hat{x}) = \int_{-\infty}^{D} p_\xi(\xi)\, d\xi = \frac{1}{2\pi j} \int_{c-j\infty}^{c+j\infty} \exp(\phi(s))\, ds, \qquad c < 0 \tag{19}$$

where

$$\phi(s) = \log(M_\xi(s)) - \log(-s) - sD. \tag{20}$$

Here $M_\xi(s)$ is the moment generating function of the random variable ξ, and the decision threshold D is equal to zero in this case because PSK signals have constant envelopes. The basis of the SAP is as follows. The above contour of integration can be moved to the left (i.e., the choice of c), provided that it does not cross any singularities of $\phi(s)$, by virtue of the Cauchy theorem [11]. Thus the choice of c is limited to the range $\text{Real}(p-) < c < 0$, where p_- is the rightmost singularity of $\phi(s)$ in the left complex plane. If a $c = c_0$ can be found such that $\phi'(c_0) = 0$ and $\phi(c_0) > 0$, then consider the vertical contour $s = c_0 + jy, -\infty < y < \infty$. Expanding the exponent $\phi(s)$ about the point $s = c_0$ in a Taylor series and neglecting higher order terms, we have

$$\phi(s) \approx \phi(c_0) - \tfrac{1}{2}\phi(c_0) y^2. \tag{21}$$

Substituting (21) into (20) and integrating along the above contour results in the expression

$$P(x \to \hat{x}) \cong \frac{1}{\sqrt{2\pi\phi(c_0)}} \exp(\phi(c_0)). \tag{22}$$

This is termed as a zeroth-order SAP [6], and c_0 is known as a saddle point of $\phi(s)$. Also, fortunately, it suffices to compute an approximate value of c_0.

Although it is possible to obtain the $M_\xi(s)$ needed in (20) using the characteristic function given in (18), we instead utilize an equivalent form (57) (see Appendix I). As will soon be evident, the use of this equivalent form of the characteristic function immediately confers a range for c_0. Equation (20) then becomes

$$\phi(s) = \sum_{i=1}^{2L} \frac{s\phi_i |\langle \eta_i \rangle|^2}{1 - 2s\phi_i} + \sum_{i=1}^{2L} \log \frac{1}{1 - 2s\phi_i} - \log(-s). \tag{23}$$

Differentiating with respect to s yields

$$\phi'(s) = \sum_{i=1}^{2L} \frac{\phi_i |\langle \eta_i \rangle|^2}{(1 - 2s\phi_i)^2} + \sum_{i=1}^{2L} \frac{2\phi_i}{1 - 2s\phi_i} - \frac{1}{s}. \tag{24}$$

Differentiating with respect to s once again yields

$$\phi(s) = \sum_{i=1}^{2L} \frac{4\phi_i^2 |\langle \eta_i \rangle|^2}{(1 - 2s\phi_i)^3} + \sum_{i=1}^{2L} \frac{4\phi_i^2}{(1 - 2s\phi_i)^2} + \frac{1}{s^2}. \tag{25}$$

We mention that the ϕ_i's are the eigenvalues of $\boldsymbol{R}^*\boldsymbol{F}$, and the η_i's are related to the means of the random variables. (Definitions of them can be found in Appendix I.) From (24), it is seen that $\phi'(c_0) = 0$ has $4L$ solutions. If ϕ_{-1} denotes the smallest negative eigenvalue of $\boldsymbol{R}^*\boldsymbol{F}$ (i.e., the one farthest away from the origin), then the solution satisfying $1/(2\phi_{-1}) < c_0 < 0$ is the only one useful to us. Examining (24) and (25) shows that when s increases from $1/(2\phi_{-1})$ to 0, $\phi'(s)$ increases from $-\infty$ to ∞, and $\phi(s) > 0$. Thus c_0 is unique and is expeditiously obtained via Newton's method. It is also apparent that this root automatically satisfies the conditions mentioned above. For the case of Rayleigh fading, the above is somewhat simplified as $\langle \eta_i \rangle = 0$.

It should be pointed out that our formulation differs from that of [4]. In [4], to find the PEP of a given error event, the error event is replaced by an equivalent error event that has the same Euclidean distance but equally weighted branches. This replacement introduces some imprecision into the estimate. Also, the method given in [4] is not suitable for the cases of nonideal interleaving and Rayleigh fading, and is only applicable to differential detection.

In sum, the following steps are needed to calculate the approximate pairwise error probability of any error event: (i) obtain $\boldsymbol{R}$ and $\boldsymbol{F}$, (ii) diagonalize both simultaneously, (iii) compute the saddle point using (24) and (25), and finally (iv) compute the approximation using (22).

B. Ideal Interleaving

For ideal interleaving/deinterleaving, the covariance matrix $\boldsymbol{R}$ (15) of $\boldsymbol{V}$ will be formed by placing R_i's diagonally, the other entries of $\boldsymbol{R}$ being zero. Thus

$$\boldsymbol{R} = \begin{pmatrix} R_1 & \cdots & 0 \\ \vdots & & \vdots \\ 0 & \cdots & R_L \end{pmatrix}. \tag{26}$$

Now, using this $\boldsymbol{R}$, the approximate PEP can be found However, in order to obtain more insight into the error performance of TCM schemes, we next derive the asymptotic behavior of this approximation. As mentioned before, it is expressed in a product form that is usable in the classical generating function method. Because of perfect interleaving/deinterleaving, the eigenvalues of $\boldsymbol{R}^*\boldsymbol{F}$ can be determined by considering each 2 $\times$ 2 matrix product $\boldsymbol{R}_i^*\boldsymbol{F}_i$. Let ϕ_{i-} and ϕ_{i+} denote those two. From (13) and (14) follows (27) (shown at the bottom of the page). Clearly, when $\mu \approx 1$ and $\sigma^2 \to 0$, we have

$$\begin{bmatrix} 1/2\phi_{i+} \\ 1/2\phi_{i-} \end{bmatrix} \approx \begin{cases} 0 \\ -\dfrac{1}{2((1-|\mu|^2)b_0+\sigma^2)}. \end{cases} \tag{28}$$

In other words, at large $\overline{E}_s/N_0$ and with reasonably accurate estimates (i.e., $\mu \approx 1$) and the $2L$ eigenvalues of $\boldsymbol{R}^*\boldsymbol{F}$ collect into two clusters, with L of them belonging to each. By substituting these in (24), it can be shown that the saddle point is given by

$$c_0 \approx -\frac{1}{4((1-|\mu|^2)b_0+\sigma^2)}. \tag{29}$$

Substituting this c_0 in (22) and manipulating further, we get

$$P(x \to \hat{x}) \cong B(L)\prod_{i=1}^{L}\frac{\Gamma}{b_0|\mu|^2|x_{k_i}-\hat{x}_{k_i}|^2+\Gamma} \cdot \exp\frac{A^2\theta|x_{k_i}-\hat{x}_{k_i}|^2}{b_0|\mu|^2|x_{k_i}-\hat{x}_{k_i}|^2+\Gamma} \tag{30}$$

where

$$B(L) \cong \frac{1}{\sqrt{2\pi(2L+1)}}$$

$$\Gamma = 4((1-|\mu|^2)b_0+\sigma^2) \tag{31}$$

$$\theta = \left[-\beta + \frac{2(b_0+b_1+\sigma^2)|\beta|^2 - 4\beta|\mu|^2 b_0}{\Gamma}\right]. \tag{32}$$

To obtain $B(L)$, the first term in (25), which can be shown to be negligible providing $\mu \approx 1$, has been neglected. In deriving θ, we have assumed, without much loss of generality, that β is real. This assumption is true for signals with symmetric spectra [12]. Also, when the quality of the channel estimates is sufficient (i.e., $\beta \approx 1, \mu \approx 1$), the value of θ is negative (≈ -0.5).

1) Ideal TC-MPSK: Here we have $\hat{\alpha}_k = \alpha_k$. Thus $b_1 = b_0, \mu = 1$, and $\beta = 1$. Substituting these values in (30) leads to the expression

$$P(x \to \hat{x}) \cong B(L)\prod_{i=1}^{L}\frac{1}{\frac{b_0}{2}|x_{k_i}-\hat{x}_{k_i}|^2\gamma_s+1} \cdot \exp\frac{-\frac{A^2}{4}|x_{k_i}-\hat{x}_{k_i}|^2\gamma_s}{\frac{b_0}{2}|x_{k_i}-\hat{x}_{k_i}|^2\gamma_s+1} \tag{33}$$

which is identical to the Chernoff upper bound (e.g. [9, (9.17)]), except the multiplier $B(L)$. For Rayleigh fading with $L = 2$, the above requires 3.7 dB less than the Chernoff bound. As shown in [2], the difference between the exact and the Chernoff bound is 3.6 dB. This fact suggests that the above approximation is quite accurate. For Rician fading channels, the accuracy of (33) decreases with increasing K.

2) TC-MDPSK: In this case, for any signaling period, the preceeding signal provides the channel estimate (7). Hence, $b_1 = b_0 + \sigma^2$, and assuming a land mobile channel [2], it follows that

$$|\mu|^2 = \frac{b_0 J_0^2(2\pi f_d T_s)}{b_0 + 0.5\gamma_s^{-1}} = \frac{b_0\delta}{b_0+0.5\gamma_s^{-1}} \tag{34}$$

where f_dT_s is the maximum normalized Doppler spread. The closer μ to unity, the more pronounced the benefits of using a code, and the better the approximation (30). Hence, we see that two factors degrade the quality of the estimates, one being the Doppler spread, and the other being the additive noise (appearing as $(\overline{E}_s/N_0)^{-1}$). Unlike pilot-aided detection, the channel estimate, being the time-delayed data signal, has the same bandwidth as the data signal. Thus even for slow fading, the additive noise degrades the quality of the estimates. In contrast, for pilot-tone-aided detection systems, as will be seen next, the pilot bandwidth approaches zero for slow fading ($f_dT_s \approx 0$), thus providing an essentially noise-free estimate.

Substituting $|\mu|^2$ in (30) results in the expression (35) given at the bottom of the next page. Once again, for Rayleigh fading ($b_0 = 0.5, A = 0$) this reduces to the Chernoff bound (e.g. [9, 9.119]) except the multiplier $B(L)$. For ideal differential detection (i.e., very slow fading) $f_dT_s \to 0, J_0(2\pi f_dT_s) \approx 1-(\pi f_dT_s)^2$, hence the approximate PEP varies as $(\pi f_dT_s)^{2L}$. This implies that the usual diversity effect of coding is applicable to the suppression of error floors as well [2]. However, this is not the case for fast fading, as (35) indicates. Note also that, unless $f_dT_s = 0$, the approximate PEP does not approach 0 as $\overline{E}_s/N_0 \to \infty$. This fact suggests the existence of error floors.

The accuracy of (35) will decrease with two increasing factors: the Doppler spread and K. From (34), it is seen that

$$\begin{bmatrix} 1/2\phi_{i+} \\ 1/2\phi_{i-} \end{bmatrix} = \frac{-b_0 \pm \sqrt{b_0^2 + 4|x_{k_i}-\hat{x}_{k_i}|^{-2}|\mu|^{-2}b_0((1-|\mu|^2)b_0+\sigma^2)}}{4b_0((1-|\mu|^2)b_0+\sigma^2)}. \tag{27}$$

for a given signal-to-noise ratio (SNR), increased K lowers the value of b_0, thereby decreasing $|\mu|^2$ as well.

3) TC-MPSK With a Pilot Tone: In practice, contrary to the convenient assumption of ideal coherent detection, the α_k's need to be measured using some technique, such as a pilot tone [2] or embedded pilot symbols [13]. Cavers and Ho [2] have analyzed the performance of TC-MPSK with a reference pilot tone over Rayleigh fading channels. Here, we obtain the error performance of this technique over Rician fading channels. To evaluate the pairwise error as given by (30), we simply need to compute the variance of $\hat{\alpha}_{k_i}$ and the covariance between $\hat{\alpha}_{k_i}$ and α_{k_i} for all k_i's. This can be accomplished by specifying the pilot-tone filter bandwidth and the fraction of power spent on the pilot tone. As in [2], the estimate $\hat{\alpha}_k$ is obtained by a pilot-tone extraction filter whose frequency response is

$$H(f) = \begin{cases} \dfrac{1}{P}, & -B_p/2 \le f \le B_p/2 \\ 0, & \text{otherwise} \end{cases} \tag{36}$$

where P is the amplitude of the pilot tone, and B_p is the bandwidth of the pilot-tone filter. Now the fraction of the total power spent on the data signal and the pilot tone is $1/(1+r)$ and $r/(1+r)$, respectively, where $r = P^2 T_s$. As mentioend in [2], the bandwidth of the pilot-tone extraction filter should be sufficiently wide to allow for undistorted measurement of the fading process. Thus $B_p = 2f_d$. Then, the output of this filter is

$$\hat{\alpha}_k = \alpha_k + \frac{\zeta_k}{P} \tag{37}$$

where ζ_k is a complex Gaussian random variable with zero mean and a variance of $B_p N_0$. It then follows that

$$\begin{aligned} \text{var}(\hat{\alpha}_k) &= b_1 \\ &= b_0 + 0.5(B_p T_s)\left(\frac{1+r}{r}\right)\gamma_s^{-1} \\ |\mu|^2 &= \frac{b_0}{b_0 + 0.5(B_p T_s)\left(\frac{1+r}{4}\right)\gamma_s^{-1}} \end{aligned} \tag{38}$$

where γ_s now accounts for the total symbol energy spent on both the data and pilot tone. The point to note here is that when $\overline{E}_s/N_0 \to \infty, |\mu|^2$ approaches unity. Thus at large SNR's, the pilot-tone technique is essentially equivalent to ideal coherent detection. By substituting this in (30), we have (39) at the bottom of the next page. Note that, unlike the case of differential detection, there doesn't exist an irreducible error floor in this case. Moreover, by neglecting the terms containing γ_s^{-1} in this and minimizing the term $[B_p T_s(1+r)/r + 1 + r]$ with respect to r, the optimum power split ratio becomes

$$r_{\text{opt}} = \sqrt{B_p T_s}. \tag{40}$$

This agrees well with the numerical values observed in [2]. As might be expected, the optimum choice of r is solely a function of the normalized, maximum Doppler. Also, by substituting r_{opt} in (39) and comparing it with (33), TCM schemes detected with a pilot tone require $10\log(1+\sqrt{B_p T_s})^2$ dB more than TCM schemes with ideal coherent detection.

C. Non-Ideal Interleaving

For a finite interleaving depth, covariance terms among different V_i's must be included in the covariance matrix $\boldsymbol{R}$ in (15). For this reason, we need to specify the covariance between α_{k_i}, and α_{k_j}:

$$\begin{aligned} r_{ij} &= \langle(\alpha_{k_i'} - \langle\alpha_{k_i'}\rangle)^*(\alpha_{k_j'} - \langle\alpha_{k_j'}\rangle)\rangle \\ &= \begin{cases} b_0 J_0(2\pi f_d T_{ij}) \\ b_0 \exp(-2\pi|T_{ij}|) \end{cases} \end{aligned} \tag{41}$$

where we have used two correlation models: Bessel and exponential [14]. T_{ij} denotes the time delay between $\alpha_{k_i'}$ and $\alpha_{k_j'}$. To find T_{ij}, we follow the method given in [3]. As mentioned previously, the interleaver scrambles the encoder output sequence as follows:

$$\begin{aligned} &\{x_1, x_2, x_3, \cdots, x_{k_i}, \cdots\} \\ &\quad \to \{x_1, x_{N_s+1}, x_{2N_d+1}, \cdots, x_{k_i'}, \cdots\} \end{aligned} \tag{42}$$

i.e., the effect of interleaving is to place the k_ith encoder output symbol in the k_i'th position of the transmitted sequence. We would like to show the mapping between k_i and $k_i', i = 1, \cdots, L$; recall that the x_{k_i}'s are the components of the transmitted codeword x that differ with those of $\hat{x}$. Assuming the x_{k_i}'s are confined to a single row of the interleaver, say the first row, we have

$$k_i' = (k_i - 1)N_d + 1, \qquad i = 1, \cdots, L. \tag{43}$$

For this assumption to be true, it is essential that the span [3] of the error event be less than the interleaving span, i.e., $k_L - k_1 + 1 \le N_s$. As in [3], we assume that (43) holds for most of the error events. Hence, the time delay between $\alpha_{k_i'}$ and $\alpha_{k_j'}$ is given by

$$T_{ij} = (k_j' - k_i')T_s = (k_j - k_i)N_d T_s. \tag{44}$$

In other words, interleaving/deinterleaving has the same effect as transmitting at a longer symbol duration $N_d T_s$ [12] or,

$$P(x \to \hat{x}) \cong B(L) \prod_{i=1}^{L} \frac{b_0(1-\delta)\gamma_s + 1 + (4b_0\gamma_s)^{-1}}{\frac{b_0}{4}\delta|x_{k_i} - \hat{x}_{k_i}|^2\gamma_s + b_0(1-\delta)\gamma_s + 1 + (4b_0\gamma_s)^{-1}} \times \exp\left\{ \frac{\frac{A^2}{4}\theta|x_{k_i} - \hat{x}_{k_i}|^2\gamma_s(1 + 0.5(b_0\gamma_s)^{-1})}{\frac{b_0}{4}\delta|x_{k_i} - \hat{x}_{k_i}|^2\gamma_s + b_0(1-\delta)\gamma_s + 1 + (4b_0\gamma_s)^{-1}} \right\}. \tag{35}$$

equivalently, as increasing the Doppler frequency by a factor of N_d [3]. Now we are in a position to evaluate the covariance between V_l and V_m $(l, m = 1, \cdots, L)$, defined as

$$r_{l,m} = \tfrac{1}{2}\langle (V_l - \langle V_l \rangle)^* (V_m - \langle V_m \rangle)^T \rangle. \tag{45}$$

For TC-MPSK, by using the definition of V_i's (10) and utilizing (41), we have

$$r_{l,m} = b_0 J_0(\rho N_d(k_m - k_l)) \cdot \begin{pmatrix} 1 & x_{km} \\ x_{k_l}^* & x_{k_l}^* x_{k_m} \end{pmatrix} \tag{46}$$

where $\rho = 2\pi f_d T_s$. Similarly for TC-MDPSK. (See (47) at the bottom of the next page.) For the exponential correlation channel model, we can simply replace the Bessel function with the exponential (41). In the case of TC-MDPSK, we have assumed, with little loss of generality, the transmitted sequence x to be the all-zero sequence.

D. Bit Error Probability

Typically, the average bit error probability of a communication system is one of the its most important performance measures. A tight upper bound on it is obtained via the union bound, which consists of infinitely many terms. Here, we use two approaches to compute the union bound. First, based on (30), it may be enumerated using a transfer function. In this case, the bit error probability of a TCM scheme with ideal interleaving/deinterleaving is upper bounded as

$$P_b \le \frac{B(L_{\min})}{k_0} \frac{\partial T(D_1, D_2, \cdots, I)}{\partial I}\bigg|_{I=1} \tag{48}$$

where k_0 is the number of input bits per encoding interval, and the D_i's are the product terms in (30), excluding $B(L)$, with each D_i being associated with $|x_{k_i} - \hat{x}_{k_i}|^2$. Note that the number of distinct D_i's is finite and that $B(L_{\min})$ is included because $B(L)$ is a decreasing function of L. The transfer function $T(D_1, D_2, \cdots, I)$ is determined by a signal flow graph having modified branch labels [15]. This bound may be strengthened by incorporating more exact (22) instead of (30) for some error events, an improvement suggested by [16].

Second, when (30) breaks down or when finite interleaving is considered, (22) must be used to compute the approximate PEP, which is not in a product form. As a result, the union bound must be truncated to include only the dominant error events. This is the approach taken in [2] to compute the bit error probability for uniform [15] TCM. The resulting approximation to the bit error probability is [2]

$$P_b \approx \frac{1}{k_0} \sum_{L_{\min}}^{N} a(x \to \hat{x})\, P(x \to \hat{x}) \tag{49}$$

where $a(x \to \hat{x})$ is the number of bit errors associated with the error event. The choice of N should not be too large, which would require an excessive amount of computation, nor too small, which would not include a sufficient number of dominant error events. $N = 4$ or 5 appears to be satisfactory for trellis codes with $L_{\min}$ 2 or 3. Also, it should be pointed out that this technique will not yield a true upper bound because of the truncation.

IV. Examples

In this section, we apply the SAP to analyze the error performance of the four state trellis-code shown in Fig. 2, which has been obtained from [15]. Cases considered are i) 4DPSK over Rician channels with either Bessel or exponential type correlation, ii) 4 PSK over Rician channels with ideal channel measurements, iii) 4DPSK over shadowed Rician channels with Bessel correlation, and iv) 4PSK over Rician channels with pilot-tone measurements. We remark that the exact PEP shown for comparison purposes in some of the results is computed by numerical integration of (17) (see Appendix II).

A. TC-4DPSK Over a Rician Channel

First of all, Fig. 3 demonstrates the accuracy of the SAP. It is clear that the SAP is extremely close to the exact value obtained by numerical integration. In Figs. 3 and 4 the interleaving depth $N_d = 16$ appears to be sufficient, while $N_d = 32$ provides better performance than ideal interleaving. This anomaly has also been observed in [3] and is attributed to the oscillatory nature of the Bessel correlation function. In contrast, for an exponential type correlation function, Figs. 5 and 6 indicate that increasing N_d always improves the bit error performance. Secondly, it is observed that an increased Rician factor K tends to reduce the interleaving loss due to insufficient N_d. This is due to the fact that for large K, the Rician channel approaches the Gaussian channel. The union upper bound on the bit error probability obtained via (35) and

$$P(x \to \hat{x}) \cong B(L) \prod_{i=1}^{L} \frac{\left[\frac{B_p T_s(1+r)}{r} + 1 + r\right] + \frac{B_p T_s (1+r)^2}{2b_0 r}\gamma_s^{-1}}{\frac{b_0}{2}|x_{k_i} - \hat{x}_{k_i}|^2 \gamma_s + \left[\frac{B_p T_s(1+r)}{r} + 1 + r\right] + \frac{B_p T_s(1+r)^2}{2b_0 r}\gamma_s^{-1}} \times \exp\left\{ \frac{\frac{A^2}{2}\theta |x_{k_i} - \hat{x}_{k_i}|^2 \gamma_s \left(1 + \frac{B_p T_s (1+r)^2}{2b_0 r}\gamma_s^{-1}\right)}{\frac{b_0}{2}|x_{k_i} - \hat{x}_{k_i}|^2 \gamma_s + \left[\frac{B_p T_s(1+r)}{r} + 1 + r\right] + \frac{B_p T_s(1+r)^2}{2b_0 r}\gamma_s^{-1}} \right\}. \tag{39}$$

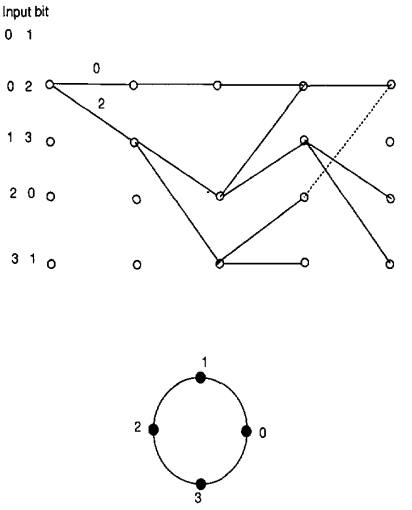

Fig. 2. Trellis diagram for 4-state, 4PSK TCM scheme [13].

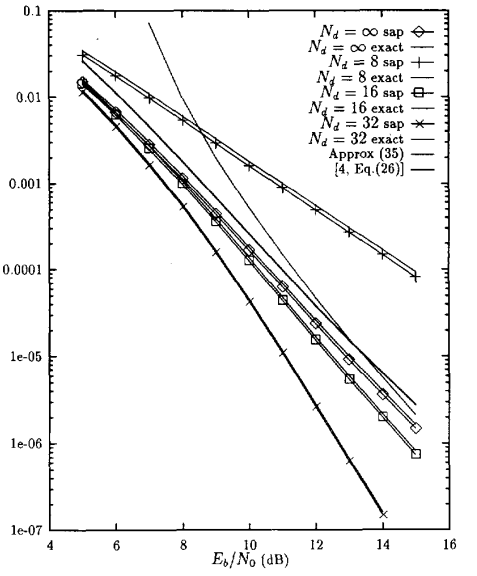

Fig. 3. Approximate bit error rate for 4-state 4DPSK TCM scheme for Rician fading with K = 5 dB. The normalized Doppler f_dT_s is 0.02 with Bessel correlation.

(48) is off by 1, 2 dB for $K = 5$, 10 dB, respectively, at large $\overline{E}_s/N_0$. For comparison purposes, the SAP given in [4] is also plotted in these figures. For $K = 10$ dB, [4, Eq. (26)] is virtually identical to the exact PEP and the SAP given in (22), as Figs. 4 and 6 show. For $K = 5$ dB, however, [4, Eq. (26)] overestimates the PEP somewhat, which may be due to the fact that the accuracy of [4, Eq. (26)] decreases with decreasing K [4].

B. TC-4PSK Over a Rician Channel

Figs. 7 through 9 show the error performance of TC-4PSK with ideal channel measurements. They again illustrate the accuracy of the SAP, which is virtually identical to the exact result obtained by numerical integration for the Rician channel. In Fig. 7, for the Rayleigh fading channel, the exact PEP's have been computed using the techniques given in [2], [3]. For ideally interleaved Rayleigh channels, the exact PEP and the SAP agree extremely well. From these figures, it is observed that the interleaving depth and the normalized Doppler spread product $N_d f_d T_s$ should be roughly about 0.3 so that the interleaver is as good as an ideal interleaver. As a point of comparison, for convolutional coded binary PSK, this product should be about 0.1 [12], [17]. Also shown is the upper bound on the bit error probability based on the Chernoff bound given in [15]. From Figs. 7, 8, and 9, the Chernoff bound is about 2 dB weaker than (33) for these cases.

C. TC-4DPSK Over a Shadowed Rician Channel

In this case, the PEP is obtained by

$$P(x \to \hat{x}) = \int_0^\infty P(x \to \hat{x}|A)\, P(A)\, dA. \qquad (50)$$

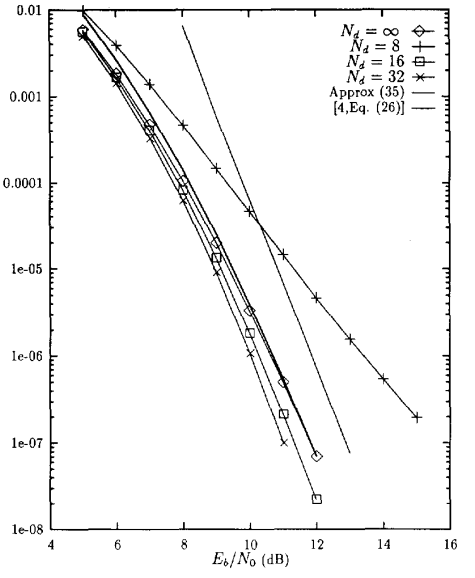

Fig. 4. Approximate bit error rate for 4-state 4DPSK TCM scheme for Rician fading with K = 10 dB. The normalized Doppler f_dT_s is 0.02 with Bessel correlation.

To compute the conditional error probability, the SAP can be used and the total integral evaluated using a numerical technique. The required interleaving depth appears to be on a par with that of Rician channels. From Figs. 10 and 11, the

$$r_{l,m} = b_0 \begin{pmatrix} J_0(\rho N_d(k_m - k_l)) & J_0(\rho(N_d(k_m - k_l) + 1)) \\ J_0(\rho(N_d(k_m - k_l) - 1)) & J_0(\rho N_d(k_m - k_l)) \end{pmatrix}. \qquad (47)$$

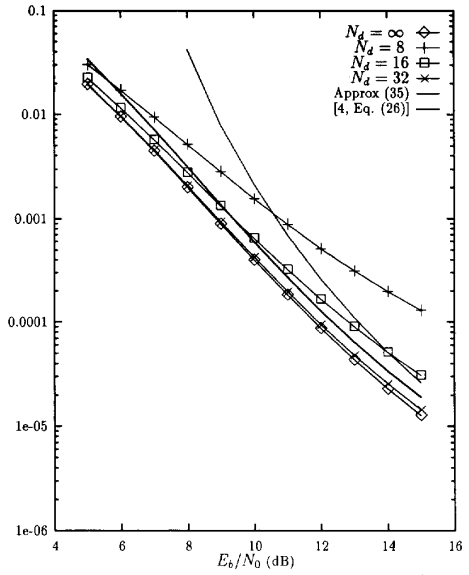

Fig. 5. Approximate bit error rate for 4-state 4DPSK TCM scheme for Rician fading with K = 5 dB. The normalized Doppler f_dT_s is 0.02 with exponential correlation.

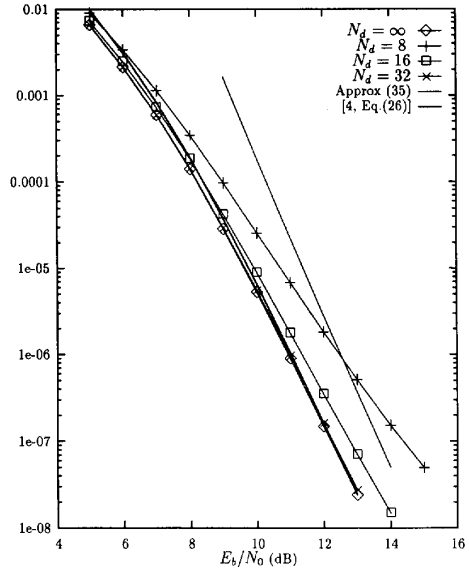

Fig. 6. Approximate bit error rate for 4-state 4DPSK TCM scheme for Rician fading with K = 10 dB. The normalized Doppler f_dT_s is 0.02 with exponential correlation.

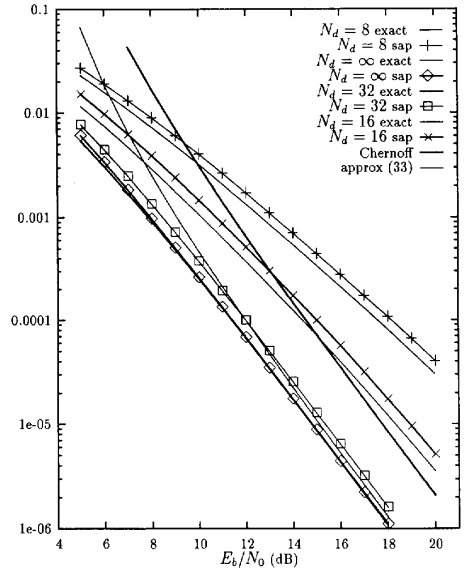

Fig. 7. Approximate bit error rate for 4-state, 4PSK TCM scheme for Rayleigh fading with K = 0. Land mobile with the normalized Doppler f_dT_s being 0.01.

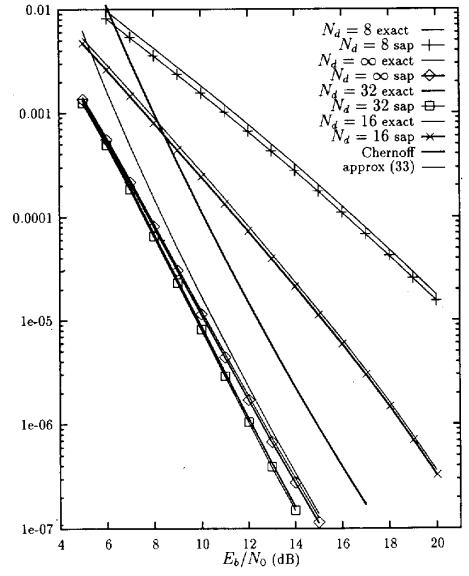

Fig. 8. Approximate bit error rate for 4-state, 4PSK TCM scheme for Rician fading, with K = 5 dB. Land mobile with the normalized Doppler f_dT_s being 0.01.

error performance of this code over both light and average shadowing channels is close to that of a 5-dB Rician channel. This observation is consistent with [4].

D. TC-4PSK With a Pilot Tone Over a Rician Channel

Fig. 12 shows the approximate bit error rate for the TC-4PSK scheme with pilot-tone-aided detection. We have considered three Doppler rates f_dT_s of 0.01, 0.03, and 0.06 and found that the corresponding optimum choice of the energy ratio r (see (40)) is 0.14, 0.25, and 0.34, respectively. This agrees well with [2]. For comparison, also shown are the performance curves of TC-4PSK with ideal channel gain measurements and TC-4DPSK for corresponding Doppler rates. It is observed that, for $f_dT_s = 0.01$, the performance of the pilot-tone technique is within 1 dB of unattainable ideal coherent detection and that it outperforms differential detection.

V. Conclusions

This paper derives an SAP for the PEP of TC-MPSK and TC-MDPSK over Rician channels. Comparison with the exact

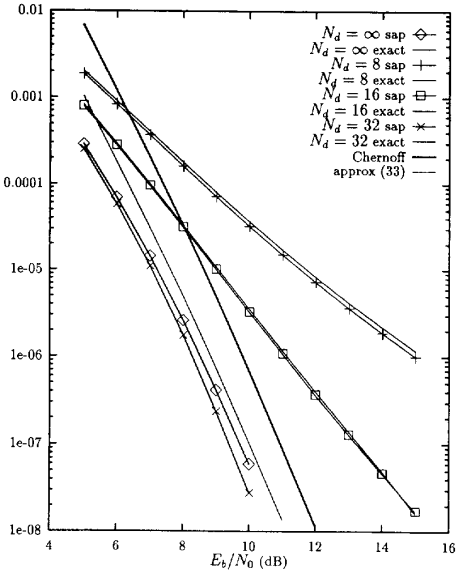

Fig. 9. Approximate bit error rate for 4-state, 4PSK TCM scheme for Rician fading, with K = 10 dB. Land mobile with the normalized Doppler f_dT_s being 0.01.

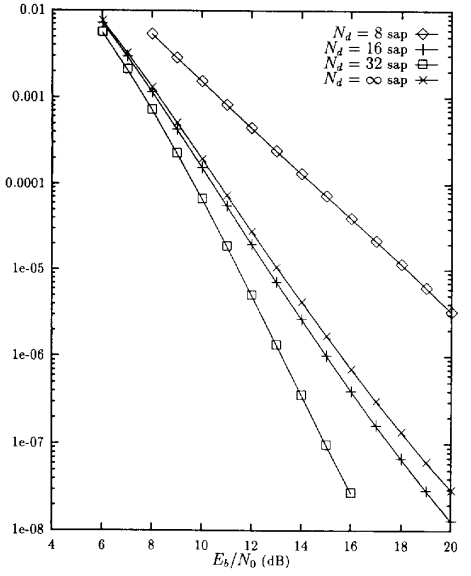

Fig. 10. Approximate bit error rate for 4-state, 4DPSK TCM scheme for light shadowed Rician fading with the normalized Doppler f_dT_s being 0.02.

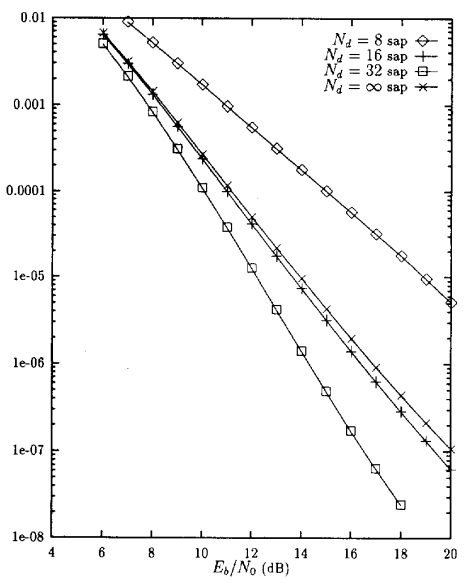

Fig. 11. Approximate bit error rate for 4-state, 4DPSK TCM scheme for average shadowed Rician fading with the normalized Doppler f_dT_s being 0.02.

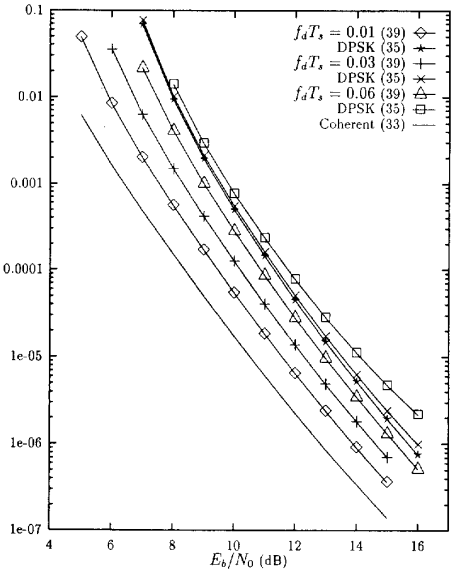

Fig. 12. Approximate bit error rate for 4-state, 4PSK TCM scheme for Rician fading with a pilot tone, K = 5 dB.

PEP computed by numerical quadrature integration indicates that the SAP is sufficiently precise (an error between 3 and 10). Incidentally, by incorporating higher order terms [6] in the saddle point method, this error can be further reduced below 1. It is felt, however, that the zeroth-order approximation will suffice for our applications. This technique may also be useful for other cases, such as trellis-coded QAM schemes [2], where one needs the probability that the decision variable is less than a certain threshold (not necessarily zero). For ideal interleaving, an asymptotic approximation of the PEP is derived which is in a product form. For nonideally interleaved Rician type channels, the performance degradation due to the finite interleaving capacity can be estimated with the help of the SAP approximation. This appears to be an extension of the work reported in [3] for the Rician model. The sufficient interleaving depth is found to be given by $N_df_dT_s \approx 0.3$. The SAP approximation alleviates the need for computer simulation for evaluating TCM bit error performance over mobile fading channels under a variety of channel models and limitations.

APPENDIX I

As mentioned before, in order to use the SAP to compute the PEP, the moment generating function of the quadratic ξ is required. For the sake of completeness, we briefly outline the steps required to obtain the characteristic functions of ξ. As shown in [10, App. B], it is possible to diagonalize $\boldsymbol{R}$ and $\boldsymbol{F}$ simultaneously. Write

$$\boldsymbol{R} = \boldsymbol{U}\boldsymbol{\Lambda}\boldsymbol{U}^{\dagger} \tag{51}$$

where $\boldsymbol{U}$ is a unitary matrix consisting of the $2L$ eignevectors of $\boldsymbol{R}$ and $\boldsymbol{\Lambda}$ is a diagonal matrix whose entries are the corresponding eigenvalues of $\boldsymbol{R}$. Since $\boldsymbol{R}$ is positive definite and hence has positive real eigenvalues, it is possible to factorize $\boldsymbol{\Lambda}$ as

$$\boldsymbol{\Lambda} = \boldsymbol{\Psi}^{*}\boldsymbol{\Psi}^{T} \tag{52}$$

where $\boldsymbol{\Psi}$ is a diagonal matrix whose entries are the square root of the eigenvalues of $\boldsymbol{R}$. Then the components of the random vector $\boldsymbol{V}$ can be made to be independent by the transformation

$$\boldsymbol{w} = \boldsymbol{\Psi}^{-1}\boldsymbol{U}^{T}\boldsymbol{V}. \tag{53}$$

With this new random vector, the Hermitian form ξ in (11) becomes $\xi = \boldsymbol{w}^{\dagger}\boldsymbol{T}\boldsymbol{w}$ where

$$\boldsymbol{T} = \boldsymbol{\Psi}^{\dagger}\boldsymbol{U}^{T}\boldsymbol{F}\boldsymbol{U}^{*}\boldsymbol{\Psi} = \boldsymbol{S}\boldsymbol{\Phi}\boldsymbol{S}^{\dagger} \tag{54}$$

since $\boldsymbol{T}$ is also Hermitian and $\boldsymbol{\Phi}$ is the diagonal matrix of its eigenvalues $\phi_i\, i = (1, \cdots, 2L)$. The transformation

$$\eta = \boldsymbol{S}^{\dagger}\boldsymbol{w} \tag{55}$$

converts the quadratic form ξ as $\xi = \eta^{\dagger}\boldsymbol{\Phi}\eta$. The mean of the random vector η is given by

$$\langle\eta\rangle = \boldsymbol{S}^{\dagger}\boldsymbol{\Psi}^{-1}\boldsymbol{U}^{T}\langle\boldsymbol{V}\rangle. \qquad hbox(56)$$

Now the characteristic function of ξ is given by [10]

$$G_{\xi}(\nu) = \prod_{i=1}^{2L} \frac{1}{1 - 2j\nu\phi_i} \exp\left[\frac{j\nu\phi_i|\langle\eta_i\rangle|^2}{1 - 2j\nu\phi_i}\right]. \tag{57}$$

This form of the characteristic function is most suitable for our application at hand, and the associated moment generating function $M_{\xi}(s)$ is obtained by making the substitution $s = j\nu$. From a computational point of view, this form requires to compute the eigenvalues and eigenvectors of the two Hermitian matrices ($\boldsymbol{R}$ and $\boldsymbol{T}$), which can be accomplished easily by the use of a software package such as MATLAB.

APPENDIX II

It is of interest to mention the method we use to evaluate the integral of (17) numerically. This method is proposed in [5] for computing certain probability distributions in optical communications. From our numerical experiments, we have found it to converge rapidly, easily yielding the desired accuracy. The basic idea is to replace the vertical contour of (17) with a sum of short contours in such a manner that the absolute value of the integrand drops off to zero as rapidly as possible. Such a contour is called the path of steepest descent [11].

From (17) and (18), write the integrand as $\exp(\Psi(s))$ with

$$\Psi(s) = s\langle\boldsymbol{V}\rangle^{\dagger}(\boldsymbol{F}^{-1} - 2s\boldsymbol{R}^{*})^{-1}\langle\boldsymbol{V}\rangle - \log\det(\boldsymbol{I} - 2s\boldsymbol{R}^{*}\boldsymbol{F}) - \log(-s). \tag{58}$$

where c_0 is chosen once again such tht $\Psi'(c_0) = 0$. Here the above contour passes through c_0 on the real axis and is parallel to the imaginary axis. As mentioned above, we can deform the above contour to construct the path of steepest descent consisting of short, straight segments of equal length $|\Delta s| = \delta$. As shown by Rice [18]

$$\Delta s = s_{k+1} - s_k = -\delta\frac{|\Psi'(s_k)|}{\Psi'(s_k)}. \tag{60}$$

$s_0 = c_0$ and the first segment is vertical. Thus

$$s_1 = s_0 + j\delta. \tag{61}$$

The initial choice of δ is given as [5]

$$\delta = \frac{1}{2\sqrt{|\Psi(s_0)|}}. \tag{62}$$

Now (59) becomes

$$P(x \to \hat{x}) = \pi^{-1}\,\mathrm{Re}\left[\sum_{k=0}^{\infty}\int_{s_k}^{s_{k+1}} \exp(\Psi(s))\,ds/j\right]. \tag{63}$$

Starting with the value of the δ above, each term of this sum can be evaluated using a five-point formula given in [5]. One can truncate this series at the k-th line segment when the contribution from the k-th term falls below the desired accuracy. Then this summation is repeated for $\delta/2$ and $\delta/4$. We have found this to yield sufficient accuracy.

REFERENCES

[1] D. Divsalar and M. K. Simon, "Trellis-coded modulation for 4800 to 9600 bps transmission over a fading satellite channel," *IEEE J. Select. Areas Commun.*, vol. JSAC-5, pp. 162–175, Feb. 1987.

[2] J. K. Cavers and P. Ho, "Analysis of the error performance of trellis-coded modulations in Rayleigh fading channels," *IEEE Trans. Commun.*, vol. 40, pp. 74–83, Jan. 1992.

[3] P. Ho and D. Fung, "Error performance of interleaved trellis-coded PSK modulations in correlated Rayleigh fading channels," *IEEE Trans. Commun.*, vol. 40, pp. 1800–1809, Dec. 1992.

[4] J. Huang and L. Campbell, "Trellis coded MDPSK in correlated and shadowed Rician fading channels," *IEEE Trans. Veh. Technol.*, vol. 40, pp. 786–797, Nov. 1991.

[5] C. W. Helstrom, "Computing the performance of optical receivers with avalanche diode detectors," *IEEE Trans. Commun.*, vol. 36, pp. 61–66, Jan. 1988.

[6] C. W. Helstrom, "Approximate evaluation of detection probabilities in radar and optical communications," *IEEE Trans. Aerosp. Electron. Syst.*, vol. 14, pp. 630–640, July 1978.

[7] K. Schumacher and J. J. O'Reilly, "Relationship between the saddle point approximation and the modified chernoff bound," *IEEE Trans. Commun.*, vol. 38, pp. 270–272, Mar. 1990.

[8] P. J. McLane *et al.*, "PSK and DPSK trellis codes for fast fading, shadowed mobile satellite communication channels," *IEEE Trans. Commun.*, vol. 36, pp. 1242–1246, Nov. 1988.

[9] M. K. Simon, E. Biglieri, P. J. McLane, and D. Divsalar, *Introduction to Trellis-Coded Modulation with Applications.* New York: McMillan, 1991.

[10] W. R. Bennet, M. Schwartz, and S. Stein, *Communication Systems and Techniques.* New York: McGraw-Hill, 1966.

[11] N. Bleistein and R. A. Handelsman, *Asymptotic Expansions of Integrals.* New York: Dover, 1986.
[12] F. Gagnon and D. Haccoun, "Bounds on the error performance of coding for non-independent Rician fading channels," *IEEE Trans. Commun.,* vol. 40, pp. 351–360, Feb. 1992.
[13] J. K. Cavers, "An analysis of pilot symbol assisted modulation for Rayleigh fading channels," *IEEE Trans. Veh. Technol.,* vol. 40, pp. 686–693, Nov. 1991.
[14] L. J. Mason, "Error probability evaluation for systems employing differential detection in a Rician fast fading environment and Gaussian noise," *IEEE Trans. Commun.,* vol. COM-35, pp. 39–46, Jan. 1987.
[15] E. Biglieri and P. J. McLane, "Uniform distance and error probability properties of TCM schemes," *IEEE Trans. Commun.,* vol. 39, pp. 41–52, Jan. 1991.
[16] R. G. Mckay *et al.,* "Error bounds for trellis-coded MPSK on a fading mobile satellite channel," *IEEE Trans. Commun.,* vol. 39, pp. 1750–1761, Dec. 1991.
[17] J. W. Modestino and S. Y. Mui, "Convolutional code performance in the Rician fading channel," *IEEE Trans. Commun.,* vol. COM-24, pp. 592–606, June 1976.
[18] S. O. Rice, "Efficient evaluation of integrals of analytic functions by the trapezoidal rule," *Bell Syst. Tech. J.,* vol. 52, pp. 707–722, 1973.

Chinthananda Tellambura was born in Anuradhapura, Sri-Lanka, on September 16, 1962. He received the B.Sc. degree in electronics and communications engineering from the University of Moratuwa, Sri-Lanka, in 1986, the M.Sc. degree in electronics from King's College, University of London, in 1988, and the Ph.D. degree in electrical engineering from the University of Victoria, Canada, in 1993..

From 1986 to 1987 and 1988 to 1989, he was an assistant lecturer at the Department of Electronic Engineering, University of Moratuwa. Presently, he is a post-doctoral fellow at the University of Victoria, BC, Canada. His current research interests include error control coding theory and mobile communications.

Qiang Wang was born in China in 1961. He received the B.Sc. and M.Sc. degrees from the Nanjing Communications Engineering Institute, Nanjing, China, in 1982 and 1985, respectively, and the Ph.D. degree from the University of Victoria, B.C., Canada, in 1988, all in electrical engineering.

From 1987 to 1990, he was a Member of the Technical Staff of Microtel Pacific Research (now MPR Teltech), Ltd., Burnaby, BC, Canada. He was involved in design and implementation of various error correction coding and modulation schemes and spread spectrum systems using DSP and VLSI technology. Since he has been an assistant professor in the Department of Electrical and Computer Engineering at the University of Victoria, while being a consultant to MPR and several other companies. His current research interests include spread spectrum communications, error control coding, and personal wireless communications.

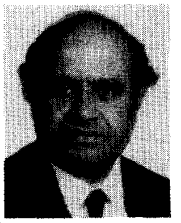

Vijay K. Bhargava (F'92) received the B.Sc. degree with honors from the University of Rajasthan in 1966, the B.Sc. degree in mathematics and engineering, and the M.Sc. and Ph.D. degrees, both in electrical engineering, from Queen's University in Kingston, ON, Canada, in 1970, 1972, and 1974, respectively.

After brief stays at the Indian Institute of Science and the University of Waterloo, he joined Concordia University in Montreal and was promoted to Professor in 1984. From 1982 to 1983, he was on sabbatical leave at \'Ecole Polytechnique de Montreal. In 1984 he joined the newly formed Faculty of Engineering at the University of Victoria as a Professor of Electrical Engineering. In 1988 he was appointed a Fellow of the BC Advanced Systems Institute. He is co-author of the book *Digital Communications by Satellite* (New York: Wiley, 1981). A Japanese translation of the book was published in 1984, and a Chinese translation was published in 1987. During 1988 to 1990, he served as the Editor of the Canadian Journal of Electrical and Computer Engineering. In 1992 he became the Director of IEEE Region 7 for a two-year term.

Dr. Bhargava is a recipient of the IEEE Centennial Medal, the EIC Centennial Medal, and the 1987 A. F. Bulgin Premium awarded by the Institute of Radio and Electronic Engineers (UK). In 1988 he was elected a Fellow of the Engineering Institute of Canada. In 1990 he received the John B. Stirling Medal of the EIC.